

Design of a Metal Oxide–Organic Framework (MoOF) Foam Microreactor: Solar-Induced Direct Pollutant Degradation and Hydrogen Generation

Liangliang Zhu, Chuan Fu Tan, Minmin Gao, and Ghim Wei Ho*

The cleaning-up of pollutant spillage and discharge is becoming increasingly important since the pollutants may have destructive environmental and ecological ramifications.^[1,2] However, there are challenges in effectively cleaning up pollutants. First, the pollutants are typically removed by absorption or skimming and then disposed of.^[3–6] Accordingly, this results in not only secondary contamination, but also leads to the absorbent material and pollutant not being recovered in an economical and useful manner. Second, recently numerous two-dimensional (2D) graphene-based foams/aerogels have been demonstrated as absorbent materials.^[7,8] In these graphene-based composites, aggregation and stacking commonly occur between individual randomly oriented nanosheets, which greatly reduces their intrinsic high specific surface area.^[9,10] Often expensive and extensive critical-point or freeze drying is needed to retain the porous interconnected-nanosheet framework. With regard to catalytic properties, reactivity loss of the graphene-based foam/aerogel is prevalent owing to impairment of physicochemical properties by defects and chemical moieties introduced during graphene oxide synthesis and reduction processes.

Here, we report the versatile synthesis of open and filled metal oxide–organic framework (MoOF) foams that are free-standing, monolithic, absorbent, and catalytic. The carbon-based absorbent foams are prepared by carbonization of a low-cost polymer precursor. The resultant three-dimensional (3D) carbon foam (CF) is seamlessly continuous with virtually non-existent intersheet junctions and defect network. We have demonstrated the adaptability of the carbon foam, in which both the interconnected fibrils and open cell pores are ideal as scaffolds for immobilization of mesoporous nanoparticles and nanosheets, leading to a composite absorber with catalytic functionalities. The open cell structure allows exceptional accessibility of reactants and the cyclable compressibility needed for

expansion/contraction during the absorption/regeneration of the foam.^[8] In essence, the carbon framework can effectively prevent undesirable nanocatalyst aggregation or release into aquatic environments and at the same time the open cell structure can cope with volume changes and alleviate mechanical stress to a certain extent. To the best of our knowledge, this is the first report of a composite combining a carbon foam with functional catalytic nanomaterials that can offer unprecedentedly effective clean-up of pollutants with a value-added function. To date, most agencies have mainly focused on treating pollutants/effluent to meet environmental discharge standards. In doing so, pollutant clean-up has only imposed costs and not produced revenue in any way. Our work demonstrates a MoOF foam that readily soaks up pollutant and localizes solar energy where photocatalysis occurs within the microreactor reservoir, leading to effective degradation and hydrogen (H₂) generation. This absorbent and solar-mediated photocatalytic foam is a promising sustainable environmental remediation solution for pollutant spill or discharged effluent.

In the design of the free-standing monolithic absorbent and catalytic foam, CF was chosen as the template for its appealing and practical attributes of light weight and effective absorption with high elastic shape recovery even after multiple cycles of large mechanical deformation.^[11,12] Moreover, it has desirable properties that complement photocatalytic processes, namely, as a conducting medium for rapid electron–hole separation and charge transport, effective solar heat absorption, and an interconnected framework with huge surface-area-to-volume ratio for fast interfacial charge transfer.^[13] The precursor of the CF is an inexpensive melamine foam (MF), which is commercially available.^[14–16] It has an interconnected network architecture and is composed of a formaldehyde and melamine resin with sodium bisulfite as an additive (Figure S1, Supporting information). The process for the preparation of the CF is simple, by means of direct carbonization of the MF in a tube furnace under a nitrogen atmosphere at a temperature of 800 °C.^[8,14] As shown in **Figure 1a**, a significant volume shrinkage of more than 70% occurs during the carbonization process, which can be attributed to the release of a large amount of nitrogen as N₂ gas and ammonia (NH₃) from the MF during the calcination. Scanning electron microscopy (SEM) images in **Figure 1b,c** reveal that the as-prepared CF inherits a similar interconnected network architecture from MF, however, with the size of the open cell and diameter of the fibrils dramatically reduced. The triangular cross section of the MF fibril transforms into concave triangular fibril structure, as shown in **Figure 1b,c** (inset). These structural modifications immensely increase the surface-area-to-volume ratio of the CF, thus bringing the contaminants and water in

Dr. L. L. Zhu, C. F. Tan, M. M. Gao, Prof. G. W. Ho
Department of Electrical and Computer Engineering
National University of Singapore
4 Engineering Drive 3, 117583, Singapore
E-mail: elehgw@nus.edu.sg

Prof. G. W. Ho
Engineering Science Programme
National University of Singapore
9 Engineering Drive 1, 117575, Singapore

Prof. G. W. Ho
Institute of Materials Research and Engineering
A*STAR (Agency for Science, Technology and Research)
3 Research Link, 117602, Singapore



DOI: 10.1002/adma.201503828

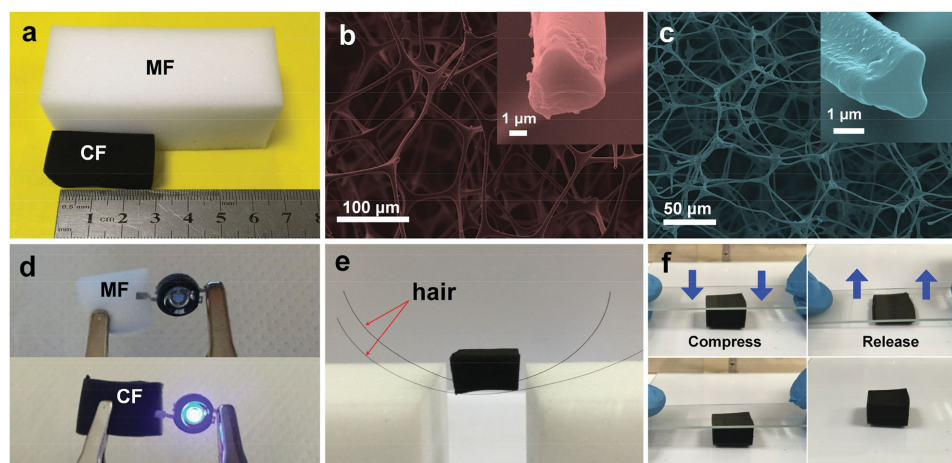


Figure 1. a) A piece of MF and the derived CF. b,c) SEM images of MF (b) and CF (c); insets: Cross-sectional image of one network fiber in the MF (b) and CF (c). d) Circuits constructed with the MF and CF as conductive bulk. e) A CF block standing on two hairs. f) Photographs of the CF under a compressing and releasing cycle.

closer proximity to the photocatalytic materials. Like many other carbon materials,^[17,18] the CF shows electrical conductivity of 2.7×10^{-3} and 2.0×10^{-4} S cm⁻¹ upon compression and release of the CF (Figure S2 and Table S1, Supporting Information). An LED can be illuminated under 6 V source when connected to an uncompressed CF (Figure 1d), which validates the adoption of CF as a catalyst support to facilitate favorable photogenerated charge transport and separation. The CF is also extremely lightweight and flexible (Figure 1e,f). It has an ultralow density of 6 ± 0.61 mg cm⁻³, which is much lower than that of the MF precursor (11 ± 0.55 mg cm⁻³) (Table S2, Supporting Information). Moreover, it is shown to retain its elastic properties, with a near complete recovery after sustaining a large compression deformation (Figure 1f). These structural and physical properties of the CF make it an excellent template medium for an absorbent catalytic foam, to complement and enhance photocatalytic processes, with appealing practical and reusable qualities.

The material compositions of MF and CF were analyzed with energy dispersive X-ray (EDX) and Fourier transform infrared (FTIR) spectrometry. The EDX spectra in Figure S3a (Supporting Information) show C, N, and O peaks at 0.26 keV, 0.39 keV, and 0.52 keV, corresponding to the composition of formaldehyde and melamine resin. Na and S peaks are seen at 1.05 keV and 2.32 keV, respectively, which stem from the sodium bisulfite additive. The relative ratio of the elements C and N increased after the calcination, indicating the nitrogen removal and carbonization process. The chemical compositions of MF and CF were also confirmed by FTIR spectra, shown in Figure S3b (Supporting Information). The spectrum of MF has absorption peaks at 3313 cm⁻¹ (ν N-H), 1537 cm⁻¹, 1454 cm⁻¹ (ν C=N), 1328 cm⁻¹ and 978 cm⁻¹ (ν C-H), 1178 cm⁻¹ (ν C-N), and 810 cm⁻¹ (bending vibration of triazine ring) (Figure S3b, black line, Supporting Information).^[19,20] In the case of CF, a broad peak was observed at 945 cm⁻¹ instead, ascribed to C-O vibration after annealing (Figure S3b, red line, Supporting Information), suggesting the presence of carbon-rich products.

The interconnected fibrils and open cell pores of the CF provide an ideal template for immobilization of photocatalytic nanomaterials. Titanium dioxide (TiO₂), a highly stable,

nontoxic, effective, and low-cost catalyst,^[21,22] was herein employed to provide photocatalytic functionalities for the MoOF foam. By using the CF as a template, two different systems, filled-cell nanoparticles (NPs) and open-cell nanosheets (NSs), have been developed, based on TiO₂ nanomaterials (Figure 2a). The SEM images of TiO₂ NP and TiO₂ NS MoOF foams are shown in Figure 2b–e. TiO₂ NP MoOF foam was synthesized by first filling up the CF with TiO₂ sol-gel. In the subsequent calcination, microblocks of MoOF were formed, with sol-gel permeation into the open cells and partitioning of the dehydrated sol along the skeleton of the CF. As a result of the micellization and evaporation of block copolymer, mesoporous TiO₂ nanoparticles were formed and filled the CF cell structure (Figure 2c), representing a large surface area for photoreactivity. On the other hand, by using the fibrils of CF as a nucleation platform, TiO₂ NSs could be uniformly grown hydrothermally. The TiO₂ NSs grew selectively on the carbon fibrils and hence preserved the open-cell structure of the CF (Figure 2d,e). The synthesis process of TiO₂ NS MoOF foam is illustrated in Figure 2f. The schematic shows the transformation of the cross section of the fibrils during the preparation of 3D TiO₂ NSs. As mentioned earlier, the triangular cross section of the fibril became concave after the sample was annealed at 800 °C in N₂. The diameter of the fibrils decreased from ca. 4 μm to ca. 2.2 μm. Subsequently, a thin layer of TiO₂ NS was grown on the surface of the concave triangular fibrils after the hydrothermal treatment at 180 °C. By further calcination at 450 °C, hollow concave triangular TiO₂ NS fibers were obtained, with a reduction in diameter to 850 nm. The corresponding SEM images are shown in the lower half of Figure 2f. The color of the foam changed from white to black, in the fabrication of CF from MF, and finally turned to white again as a result of formation of TiO₂, as shown in Figure S4 (Supporting Information). The transmission electron microscopy (TEM) images of TiO₂ NP and TiO₂ NS MoOF foams are shown in Figures S5a,b and S5d,e (Supporting Information), respectively. It could be seen that the TiO₂ NP MoOF foam was composed of interconnected mesoporous NPs (Figure S5a, Supporting Information). The clear lattice spacing of 0.352 nm observed in Figure S5b (Supporting Information)

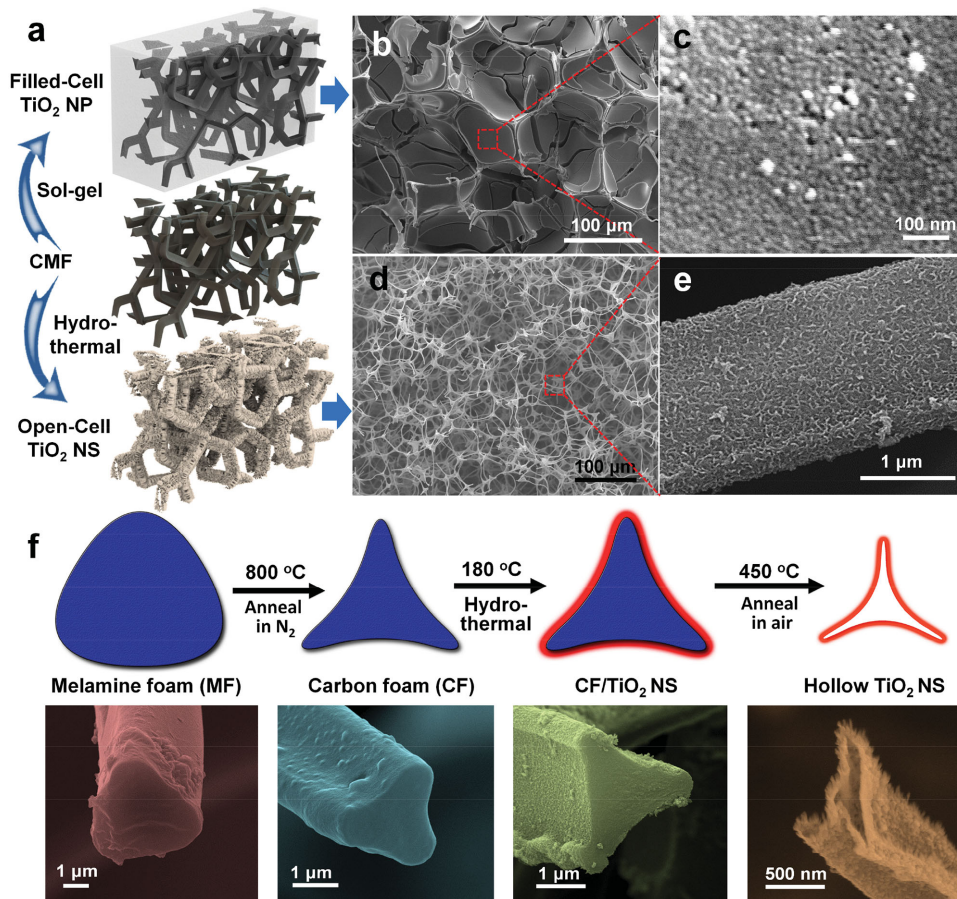


Figure 2. a) Schematic illustration of synthesis of TiO₂ MoOF foam. b–e) SEM images of TiO₂ NP MoOF foam (b,c) and TiO₂ NS MoOF foam (d,e). f) Formation procedure of TiO₂ NS MoOF foam.

is in agreement with the values for the (101) lattice planes of tetragonal anatase TiO₂.^[23,24] The hollow fibers in TiO₂ NS MoOF shown in Figure S5d (Supporting Information) are made up of a thin layer of TiO₂ NSs (Figure S5b, Supporting Information), which is consistent with the result of SEM images.

To further enhance the photocatalytic performance of the foam, copper oxide (CuO), of narrower bandgap, was introduced into the TiO₂ and TiO₂/CuO MoOF foams as an efficient co-catalyst by a simple wet impregnation method.^[23,25–27] The high-resolution TEM images of TiO₂ NP/CuO and NS/CuO MoOF foams are presented in Figure S5c,f (Supporting Information). The lattice fringe of 0.232 nm corresponding to the (111) plane of CuO is observed, confirming the formation of a composite with CuO in the TiO₂.^[23] X-ray diffraction (XRD) spectra were employed to determine the crystal structures of as-prepared TiO₂ and TiO₂/CuO MoOF foams (Figure 3a). The diffraction peaks in the spectra of both TiO₂ NP and TiO₂ NS MoOF foams at 25.36°, 37.91°, 38.70°, 48.15°, 54.07°, 55.18°, 62.81°, 68.84°, 70.35°, and 75.27° can be indexed to the (101), (004), (112), (200), (105), (211), (204), (116), (220), and (215) crystal planes of the anatase phase of TiO₂, respectively.^[23,28] The crystalline peak that appears at $2\theta = 35.5^\circ$ corresponds to the CuO crystalline structure. The EDX spectra in Figure 3b show clear Ti peaks at 4.51 and 4.95 keV. The Cu peaks at 0.93 and 8.05 keV indicate that the CuO nanoparticles

were successfully incorporated into the TiO₂ NP and TiO₂ NS MoOF foams.^[25,29] X-ray photoelectron spectroscopy (XPS) analysis was also adopted to determine the chemical states of the TiO₂ NP/CuO MoOF foams, particularly for Ti and Cu. The wide scan spectrum in Figure 3c shows the binding energy peaks at 285.0, 459.1, 530.1, and 935.4 eV, which are attributed to C 1s, Ti 2p, O 1s, and Cu 2p, respectively. Binding energies of 458.6 and 464.4 eV are indicative of Ti 2p_{3/2} and Ti 2p_{1/2}, with the Ti 2p spectrum (Figure 3d) corresponding to the Ti⁴⁺ tetragonal structure.^[30] Meanwhile, the peak at 530.1 eV provides evidence of O 1s in TiO₂ and CuO (Figure 3e). The Cu 2p peak is shown in Figure 3f. The Cu 2p_{3/2} is located at 934.6 eV with a shakeup satellite peak at about 943.6 eV and Cu 2p_{1/2} at 954.1 eV. The presence of shakeup satellite features for Cu 2p rules out the possibility of the presence of Cu₂O phase. The gap between Cu 2p_{1/2} and Cu 2p_{3/2} is about 20 eV, which is in agreement with the standard CuO spectrum.^[31,32]

The performance of MoOF foams was first investigated for H₂ production based on photocatalytic sacrificial water splitting in a suspension.^[33,34] In this case, it was found that the H₂ evolution rate can be enhanced, compared to Degussa P25 TiO₂, by the 3D interconnected structures and introduction of CuO as co-catalyst. Figure 4a,b illustrates the time evolution of H₂ for P25, TiO₂, and TiO₂/CuO MoOF foam. P25 TiO₂, which was used as the control sample, shows a H₂ evolution rate of about 70.3 μmol g⁻¹ h⁻¹

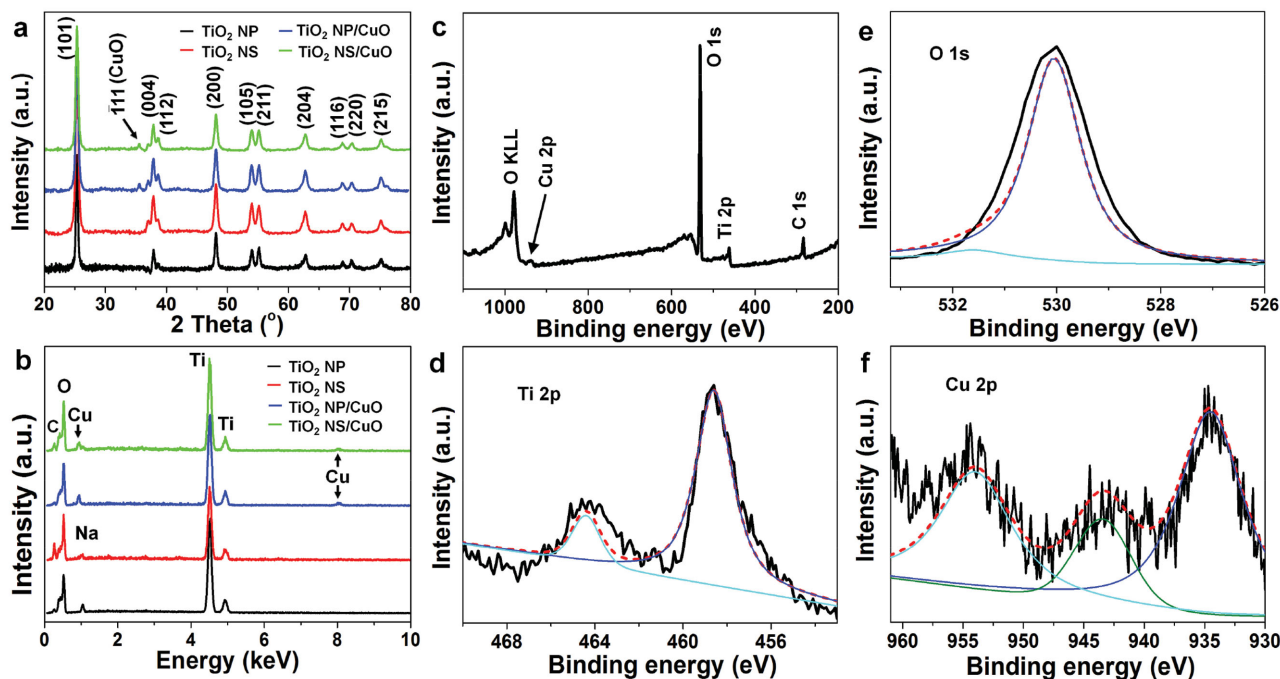


Figure 3. XRD (a) and EDX (b) spectra of TiO_2 and TiO_2/CuO MoOF foam. c) XPS spectrum of TiO_2 NP/ CuO MoOF foam. d–f) High-resolution XPS spectra of TiO_2 NP/ CuO MoOF foam for Ti 2p (d), O 1s (e), and Cu 2p (f).

(black), while TiO_2 NP and TiO_2 NS MoOF foams have much higher evolution rates of 243.8 and 177.1 $\mu\text{mol g}^{-1} \text{h}^{-1}$, respectively. The enhancement can be attributed to the 3D porous structures, consisting of pores of different scales, from mesopores to macropores, that provide a combination of high specific surface area and open channels for efficient diffusion of reactants. Further

improvement of H_2 generation was achieved after CuO co-catalyst was introduced into the TiO_2 photocatalyst and optimized by adjusting the content of CuO (Figure 4c). The amount of H_2 evolved increased with CuO content up to 3 wt%. The highest H_2 evolution rates were 556.9 and 281.8 $\mu\text{mol g}^{-1} \text{h}^{-1}$ for TiO_2 NP/ CuO and TiO_2 NS/ CuO MoOF foams, which are about 8 and

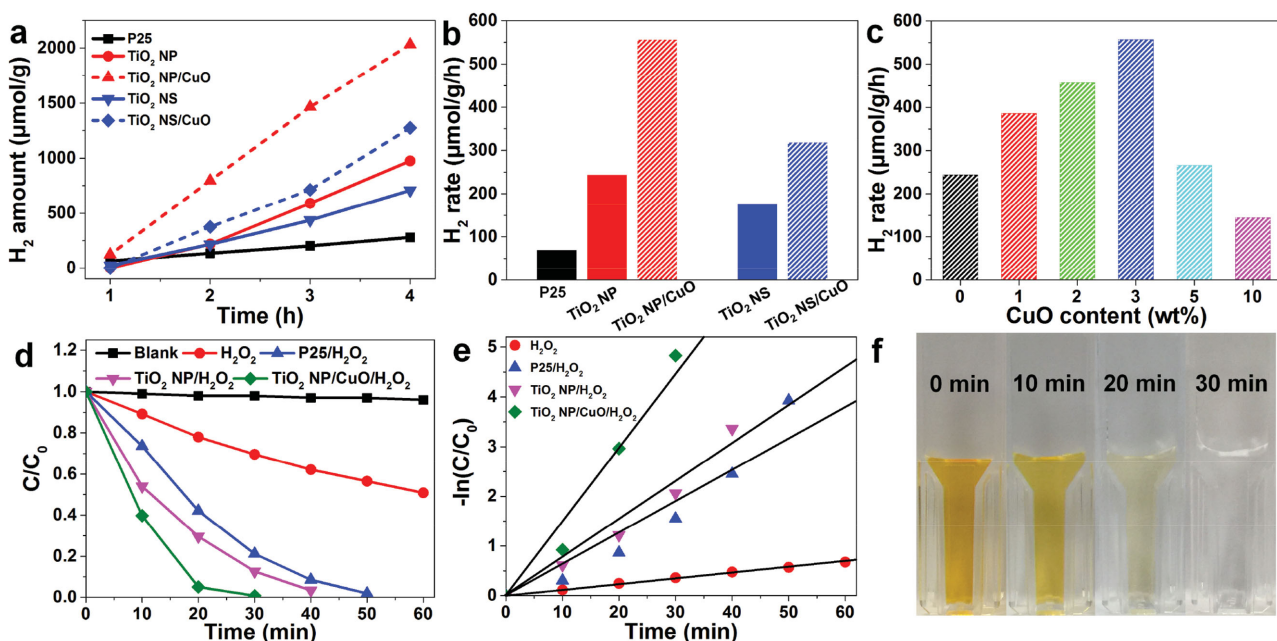


Figure 4. a) H_2 evolution as a function of irradiation time. b) H_2 rates for P25 TiO_2 , TiO_2 , and TiO_2/CuO MoOF foam. c) H_2 rates for different CuO contents. Degradation kinetics (d) and pseudo-first-order kinetics (e) of time evolution MO photodegradation study in the absence and presence of TiO_2 NP and TiO_2 NP/ CuO MoOF foam. f) Illustration of the time evolution of MO photodegradation using TiO_2 NP/ CuO MoOF foam.

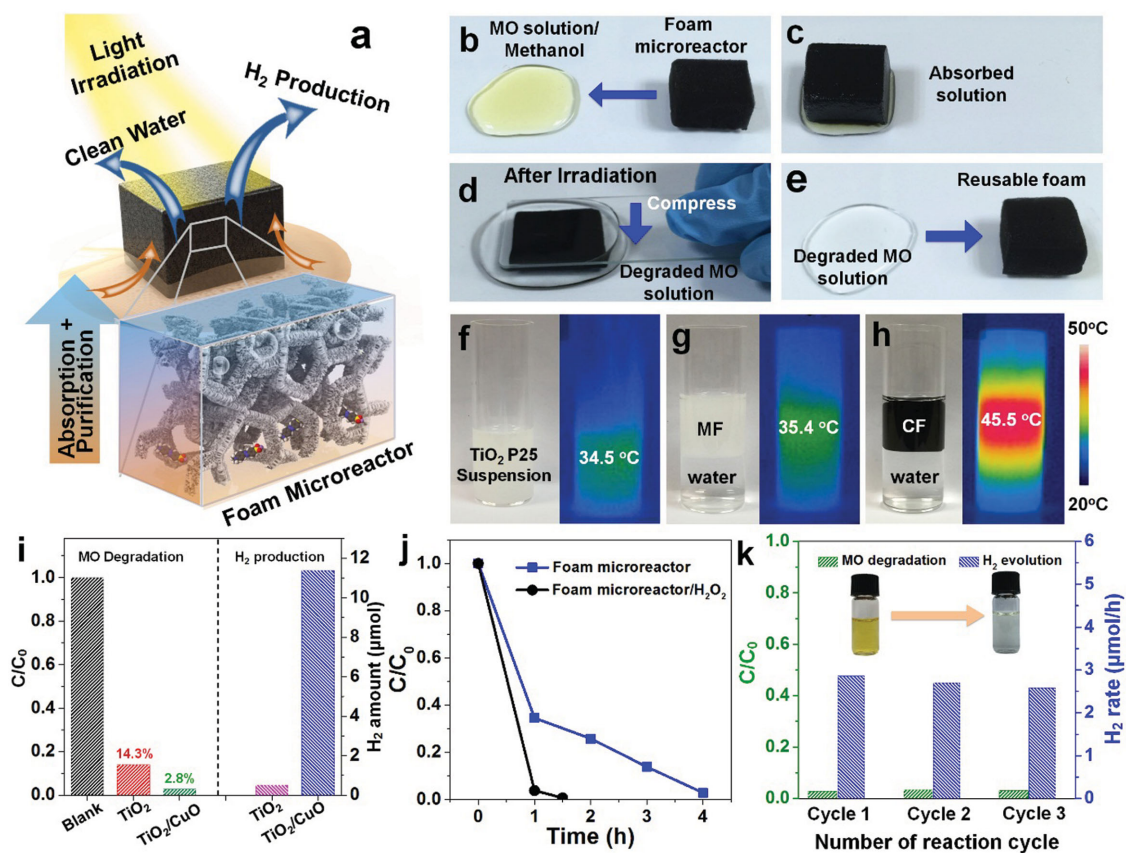


Figure 5. a) Schematic illustration of photocatalytic reaction in MoOF foam microreactor. b–e) Process of MO degradation and H₂ production: Foam absorbs MO aqueous/methanol solution (b,c). Clear water that was squeezed out after photocatalysis (d,e). f–h) Digital and infrared images of TiO₂ P25 suspension (5 mg TiO₂ P25 in 10 mL DI water) (f), MF soaked in DI water (g), CF soaked in DI water under the Xe arc lamp (h). i) MO removal (%) and H₂ evolution in TiO₂ and TiO₂/CuO MoOF foam microreactor after 4 h irradiation. j) Degradation kinetics of time evolution MO photodegradation study in TiO₂/CuO MoOF foam microreactor with and without H₂O₂. k) Reusability for degradation and H₂ production by TiO₂/CuO MoOF foam microreactor. Inset: Illustration of MO degradation.

4 times that of P25 TiO₂, respectively. Furthermore, the photocatalytic performance of TiO₂ NP/CuO MoOF foam was also tested by means of photocatalytic degradation of methyl orange (MO), a common textile dye pollutant.^[23,35] Figure 4d shows the degradation of MO in the absence and presence of different photocatalysts, with a control experiment that indicates that photodegradation is not apparent without the use of any catalytic material or H₂O₂.^[36,37] With H₂O₂, the result shows 49.1% degradation of the MO dye after 60 min. In contrast, the full degradation capabilities of P25 TiO₂, TiO₂ NP and TiO₂ NP/CuO MoOF foam were tested and shown to degrade the MO molecules after 50, 40, and 30 min of UV–vis irradiation, respectively. TiO₂ NP/CuO MoOF foam displayed the highest photocatalytic activity for MO degradation, as shown in the corresponding digital photographs (Figure 4f). Figure 4e shows the pseudo-first-order kinetics of the MO degradation of the various photocatalysts. The efficiency of MO photodegradation by the composites was determined quantitatively using the pseudo-first-order model:^[38]

$$\ln(C_t/C_0) = -kt \quad (1)$$

where C_0 and C_t are the concentrations of dye at time 0 and t , respectively, and k is the pseudo-first-order rate constant. The

constants k of P25 TiO₂, TiO₂ NP, and TiO₂ NP/CuO MoOF foam are 0.0631, 0.0765, and 0.1487 min⁻¹, respectively. The results clearly prove that the MoOF foam exhibits enhanced photodegradation compared to P25 TiO₂.

By adjusting the annealing atmosphere and temperature during the preparation of the TiO₂ NS MoOF foam, a 3D MoOF foam absorber and catalytic microreactor has been developed. Brunauer–Emmett–Teller (BET) measurements obtained from the MoOF foam microreactor gave a specific surface area of 41.18 m² g⁻¹, pore size range of 2–4 nm, and a total pore volume of 0.11 cm³ g⁻¹ (Figure S6, Supporting Information). The MoOF foam microreactor utilizes both absorption and shape recovery properties of the CF to soak up spill-polluted or waste water and to perform photocatalysis within the microreactor itself. This results in the creation of a simple and straightforward photodegradation and H₂-generation system that is self-contained and lightweight and does not require an expensive and fragile quartz photoreactor setup. The skeleton and open-cell structures in the CF are preserved in its fabrication, with the annealing in N₂. Due to the hydrophilic TiO₂ coating on its skeleton, the MoOF foam microreactor soaks up polluted water readily. Figure 5a schematically illustrates the absorption process and photocatalytic reaction of the MoOF foam microreactor,

which is distinctively different from the conventional photocatalysis setup. Traditionally, such photocatalytic reactions are carried out in a liquid-phase solution with the subsequent addition of photocatalyst in powder form.^[39,40] Mechanical stirring is often required in the suspension system, to ensure that the powdered photocatalyst is able to mix and interface well with the reagent. In contrast, the fabricated microreactor channels the reactants directly into its open cells through the absorption process, in close proximity to the photocatalytic material, thus eliminating the need for any form of mechanical mixing or liquid containment. This has simplified the reaction setup, offering convenience in its practical utilization and making many more applications feasible. MO aqueous/methanol (50:50, v/v) solution was used to determine the photocatalytic performance of the TiO₂ MoOF foam microreactor, the procedure for which is shown in Figure 5b–e. A foam reactor of size of 18 mm × 15 mm × 10 mm was saturated with the pollutant and then irradiated with UV light. After some time, the MO was degraded successfully and a colorless transparent solution was expelled from the system by simply compressing the foam microreactor (Figure 5d). Moreover, the reactor is able to return to its original form after the entire process (Figure 5e), implying a favorable reusability. We also demonstrated that the photocatalytic activity can be immensely enhanced by introducing CuO into the TiO₂ MoOF foam microreactor. Figure 5f shows the MO degradation rate and H₂ production of TiO₂ and TiO₂/CuO MoOF foam microreactors. After photo-irradiation for 4 h, the degradation of MO is approximately 85.7% and 97.2% for TiO₂ and TiO₂/CuO MoOF foam microreactors, respectively. Meanwhile, the H₂ evolution of TiO₂/CuO MoOF foam microreactor was up to 11.38 μmol, which is 21.9 times that of the TiO₂ MoOF foam microreactor (Figure 5i and Figure S7, Supporting Information). Similar to MoOF foams, H₂O₂ also promotes the photodegradation property of the microreactor; MO degradation time shortened to 1.5 h (Figure 5j). Furthermore, it is shown that the foam microreactor effectively absorbs solar heat to raise the temperature. This will further enhance the photocatalytic performance, using heat in addition to incident light radiation.^[41,42] Comparing the infrared images of TiO₂ P25 suspension, MF and CF systems under the same duration of xenon lamp irradiation, we found that CF exhibits the highest increment in temperature. The temperature attained by CF is 45.5 °C after simulated solar light irradiation for 5 min, as compared to 34.5 °C for TiO₂ P25 suspension and 35.4 °C for MF (Figure 5f–h). Moreover, to determine the reusability of the foam microreactor, MO degradation and H₂ generation by TiO₂/CuO MoOF foam microreactor were carried out for a few cycles. As shown in Figure 5k, no obvious loss of photocatalytic performance was observed and the end product from every cycle is colorless and transparent (Figure 5k, inset). A foam microreactor of size 30 mm × 16 mm × 12 mm was irradiated for 32 h continuously with purging every 8 h by argon gas, hence indicating the potential in long-term photocatalytic reactions (Figure S8, Supporting Information). This demonstrates the structural stability of the foam microreactor and its suitability for practical applications as a self-contained, monolithic absorbent and catalytic foam.

In summary, we have designed and demonstrated a facile template method to fabricate a hierarchically structured 3D

MoOF foam microreactor with photocatalytic properties for simultaneous application in solar H₂ evolution and pollutant degradation. The CF with a 3D interconnected network of high elasticity and ultra-lightweight properties is obtained by the direct carbonization of MF. Using the CF as a template, 3D mesoporous TiO₂ NP and hollow TiO₂ NS MoOF foams were developed. Furthermore, TiO₂ MoOF foam microreactors were developed and a new route to self-contained H₂ production and organic waste degradation was demonstrated. The MoOF foam microreactor readily soaks up contaminated water and performs photocatalysis within itself. This new MoOF foam microreactor and unique mode of simultaneous H₂ production and pollutant degradation is a promising, sustainable environmental remediation solution for pollutant spill or discharged effluent.

Experimental Section

Materials: All chemicals were purchased from commercial suppliers and used without further purification. Melamine foam (MF) was obtained from DAISO (Singapore). Pluronic P123, copper acetate (Cu(Ac)₂), tetrabutyl titanate (TBT), methyl orange (MO), hydrochloric acid (HCl), hydrogen peroxide (H₂O₂, 30%), dimethylformamide (DMF), isopropyl alcohol (IPA), methanol, and ethanol were purchased from standard sources.

Preparation of CF: The MFs were put into an electric furnace and heated to 800 °C with a heating rate of 5 °C min⁻¹ under a nitrogen atmosphere. The annealing process took place for 2 h at the final temperature to finish the carbonization. The as-prepared CF was then cooled down to room temperature.

Synthesis of the TiO₂ NP and TiO₂ NP/CuO MoOF Foam: TiO₂ NP MoOF foam was prepared by a sol-gel process. First, the TiO₂ sol-gel was prepared. In a typical run, 5.35 g TBT and 3.2 g HCl were added to 10 g of ethanol. 1 g of P123 was added dropwise while the solution was stirred at 400 rpm. The as-prepared solution was aged at 13 °C for 2 days after 2 h of stirring. The CF bulk with a size of about 20 mm × 15 mm × 10 mm was then immersed into the mixed precursor solution. After the solvent evaporation, the annealing treatment for CF/TiO₂ sol-gel was conducted at 450 °C for 2 h. TiO₂ NP/CuO MoOF foam photocatalyst was subsequently synthesized by introducing CuO into TiO₂ NP MoOF foam photocatalyst by a wet deposition method. The amount of CuO incorporated was 1, 2, 3, 5, and 10 wt%, respectively.

Synthesis of the TiO₂ NS and TiO₂ NS/CuO MoOF Foam: TiO₂ NS MoOF foam photocatalyst was prepared by a hydrothermal process. The precursor solution was prepared by dissolving a certain amount of TBT into 25 mL mixed solvent of 20 mL IPA and 5 mL DMF. The CF bulk with a size of about 20 mm × 15 mm × 10 mm was then immersed into the mixed precursor solution. The hydrothermal treatment was subsequently conducted at 180 °C for 12 h. After the reactions, the products were washed with IPA and dried at 55 °C. Finally, the as-prepared CF/TiO₂ composite was calcinated in air at 450 °C for 2 h. TiO₂ NS/CuO MoOF foam was fabricated using the same method as the TiO₂ NS MoOF foam.

Characterizations: Crystallographic information about the fabricated products was obtained using X-ray diffraction (XRD, Philips X-ray diffractometer with Cu K α radiation at $\lambda = 1.541 \text{ \AA}$). Morphology and structural characteristics were studied using field-emission scanning electron microscopy (FESEM, JEOL FEG JSM 7001F). The elements were analyzed by energy-dispersive X-ray spectroscopy (EDX, Oxford Instruments). The crystal structure of the composite was investigated by using transmission electron microscopy (TEM, Philips FEG CM300), at 200 kV, and X-ray photoelectron spectroscopy (XPS, VG Thermo Escalab 2201-XL). Infrared images were captured using a FLIR i60 infrared camera. Brunauer–Emmett–Teller (BET, Quantachrome Nova 2200)

measurements were conducted with nitrogen (N₂) as the adsorbate at liquid nitrogen temperature.

Photocatalytic Testing of TiO₂ and TiO₂/CuO MoOF Foam: 2 mg of photocatalyst, 9 mL deionized (DI) water and 1 mL methanol were mixed in a 25 mL quartz cylindrical reaction cell and stirred for 30 min to form a homogeneous suspension. The reactor was purged with argon (Ar) gas for 10 min prior to illumination with a 300 W xenon arc lamp of intensity 100 mW cm⁻². Gas samples were analyzed using gas chromatography (Shimadzu GC-2014AT).

The photocatalytic reactions of 15 mL aqueous solution (20 mg L⁻¹) with additional 0.5 mL H₂O₂ was carried out based on 5 mg of P25 TiO₂, TiO₂ NP, and TiO₂ NP/CuO MoOF foam under irradiation from the same Xe arc lamp. The concentration of MO was analyzed using a UV-vis spectrophotometer (Shimadzu UV-3600) and the maximal absorbance peak value was noted to plot the amount of MO degraded and, thus, to determine the photodegradation activity of the composite.

Preparation of MoOF Foam Microreactor and Photocatalytic Testing: The TiO₂ MoOF foam microreactor was fabricated as described in the synthesis of the TiO₂ NS MoOF foam except for the calcination process in N₂. The TiO₂/CuO MoOF foam microreactor was synthesized by annealing the TiO₂ MoOF foam microreactor at 300 °C in air for 2 h followed by soaking up Cu(Ac)₂ ethanol solution with the concentration of 0.00125 mol L⁻¹.

The foam reactor of dimensions 18 mm × 15 mm × 10 mm was saturated with mixed solutions (Mixed solution without H₂O₂: 20 mg L⁻¹ MO aqueous solution/methanol, 50:50 v/v; mixed solution with H₂O₂: 0.5 mL H₂O₂ was added to the 15 mL mixed solution without H₂O₂) and then transferred to a 25 mL quartz cylindrical tube. The quartz tube was purged with argon (Ar) gas for 10 min prior to illumination with UV light. The concentrations of MO and H₂ were analyzed as described above.

Supporting Information

Supporting Information is available from the Wiley Online Library or from the author.

Acknowledgements

This work is supported by MOE R-263-000-B38-112/R-263-000-B63-112 and NRF R-263-000-B82-279.

Received: August 6, 2015

Revised: September 23, 2015

Published online: October 26, 2015

- [1] R. C. Hale, M. J. La Guardia, E. P. Harvey, M. O. Gaylor, T. M. Mainor, W. H. Duff, *Nature* **2001**, 412, 140.
- [2] W. W. Lei, D. Portehault, D. Liu, S. Qin, Y. Chen, *Nat. Commun.* **2013**, 4, 1777.
- [3] P. Calcagnile, D. Fragouli, I. S. Bayer, G. C. Anyfantis, L. Martiradonna, P. D. Cozzoli, R. Cingolani, A. Athanassiou, *ACS Nano* **2012**, 6, 5413.
- [4] H. J. Zhao, X. F. Song, H. B. Zeng, *NPG Asia Mater.* **2015**, 7, e168.
- [5] Z. J. Wu, L. J. Kong, H. Hu, S. H. Tian, Y. Xiong, *ACS Sustainable Chem. Eng.* **2015**, 3, 552.
- [6] J. Li, X. Xiao, X. W. Xu, J. Lin, Y. Huang, Y. M. Xue, P. Jin, J. Zou, C. C. Tang, *Sci. Rep.* **2013**, 3, 3208.
- [7] H. Y. Sun, Z. Xu, C. Gao, *Adv. Mater.* **2013**, 25, 2554.
- [8] S. Chen, G. He, H. Hu, S. Jin, Y. Zhou, Y. He, S. He, F. Zhao, H. Hou, *Energy Environ. Sci.* **2013**, 6, 2435.
- [9] Y. A. Samad, Y. Q. Li, A. Schiffer, S. M. Alhassan, K. Liao, *Small* **2015**, 11, 2380.
- [10] X. Wang, Y. Zhang, C. Zhi, X. Wang, D. Tang, Y. Xu, Q. Weng, X. Jiang, M. Mitome, D. Golberg, Y. Bando, *Nat. Commun.* **2013**, 4, 2905.
- [11] Z. P. Chen, C. Xu, C. Ma, W. Ren, H. M. Cheng, *Adv. Mater.* **2013**, 25, 1296.
- [12] S. J. He, H. Q. Hou, W. Chen, *J. Power Sources* **2015**, 280, 678.
- [13] K. Lafdi, O. Mesalhy, A. Elgafy, *Carbon* **2008**, 46, 159.
- [14] L. Shen, J. Wang, G. Xu, H. Li, H. Dou, X. Zhang, *Adv. Energy Mater.* **2015**, 5, 1400977.
- [15] X. L. Huang, D. Xu, S. Yuan, D. L. Ma, S. Wang, H. Y. Zheng, X. B. Zhang, *Adv. Mater.* **2014**, 26, 7264.
- [16] J. S. Lee, G. S. Park, S. T. Kim, M. L. Liu, J. Cho, *Angew. Chem. Int. Ed.* **2013**, 125, 1060.
- [17] M. Q. Yang, N. Zhang, M. Pagliaro, Y. J. Xu, *Chem. Soc. Rev.* **2014**, 43, 8240.
- [18] X. Xie, G. Yu, N. Liu, Z. Bao, C. S. Criddle, Y. Cui, *Energy Environ. Sci.* **2012**, 5, 6862.
- [19] D. J. Merline, S. Vukusic, A. A. Abdala, *Polym. J.* **2013**, 45, 413.
- [20] W. Y. Zhang, H. J. Huang, F. Li, K. M. Deng, X. Wang, *J. Mater. Chem. A* **2014**, 2, 19084.
- [21] T. Kawai, T. Sakata, *Nature* **1979**, 282, 283.
- [22] W. L. Ong, M. M. Gao, G. W. Ho, *Nanoscale* **2013**, 5, 11283.
- [23] L. L. Zhu, M. H. Hong, G. W. Ho, *Nano Energy* **2015**, 11, 28.
- [24] W. Q. Wu, H. S. Rao, Y. F. Xu, Y. F. Wang, C. Y. Su, D. B. Kuang, *Sci. Rep.* **2013**, 3, 1892.
- [25] J. Bandara, C. P. K. Udawatta, C. S. K. Rajapakse, *Photochem. Photobiol. Sci.* **2005**, 4, 857.
- [26] C. K. N. Peh, M. M. Gao, G. W. Ho, *J. Mater. Chem. A* **2015**, 3, 19360.
- [27] G. Li, N. M. Dimitrijevic, L. Chen, T. Rajh, K. A. Gray, *J. Phys. Chem. C* **2008**, 112, 19040.
- [28] W. X. Guo, F. Zhang, C. J. Lin, Z. L. Wang, *Adv. Mater.* **2012**, 24, 4761.
- [29] S. I. In, D. D. Vaughn, R. E. Schaak, *Angew. Chem. Int. Ed.* **2012**, 51, 3915.
- [30] X. Q. Qiu, M. Miyauchi, K. Sunada, M. Minoshima, M. Liu, Y. Lu, D. Li, Y. Shimodaira, Y. Hosogi, Y. Kuroda, K. Hashimoto, *ACS Nano* **2012**, 6, 1609.
- [31] S. S. Lee, H. W. Bai, Z. Y. Liu, D. D. Sun, *Appl. Catal. B* **2013**, 140, 68.
- [32] M. A. Dar, S. H. Nam, Y. S. Kim, W. B. Kim, *J. Solid State Electrochem.* **2010**, 14, 1719.
- [33] S. J. Moniz, S. A. Shevlin, D. J. Martin, Z. X. Guo, J. Tang, *Energy Environ. Sci.* **2015**, 8, 731.
- [34] Z. G. Zou, J. H. Ye, K. Sayama, H. Arakawa, *Nature* **2001**, 414, 625.
- [35] L. L. Zhu, M. H. Hong, G. W. Ho, *Sci. Rep.* **2015**, 5, 11609.
- [36] T. X. Wu, G. M. Liu, J. C. Zhao, H. Hidaka, N. Serpone, *J. Phys. Chem. B* **1999**, 103, 4862.
- [37] M. Cheng, W. Ma, J. Li, Y. Huang, J. Zhao, Y. X. Wen, Y. M. Xu, *Environ. Sci. Technol.* **2004**, 38, 1569.
- [38] J. M. Herrmann, H. Tahiri, Y. Ait-Ichou, G. Lassaletta, A. R. Gonzalez-Elipe, A. Fernandez, *Appl. Catal. B* **1997**, 13, 219.
- [39] A. Kudo, Y. Miseki, *Chem. Soc. Rev.* **2009**, 38, 253.
- [40] K. Maeda, K. Teramura, D. Lu, T. Takata, N. Saito, Y. Inoue, K. Domen, *Nature* **2006**, 440, 295.
- [41] M. Matsuoka, Y. Die, M. Ogawa, *Phys. Chem. Chem. Phys.* **2014**, 16, 3520.
- [42] N. Barka, S. Qourzal, A. Assabbane, A. Nounah, Y. Ait-Ichou, *J. Photochem. Photobiol. A* **2008**, 195, 346.